Sr V-VI line widths in hot white dwarf atmospheres

Rihab Aloui, Haykel Elabidi, Sylvie Sahal-Bréchot

Monthly Notices of the ROYAL ASTRONOMICAL SOCIETY

MNRAS **512,** 1598–1607 (2022) https://doi.org/10.1093/mnras/stac405
Advance Access publication 2022 February 22

Sr V–VI line widths in hot white dwarf atmospheres

Rihab Aloui,[1]★ Haykel Elabidi [2]★ and Sylvie Sahal-Bréchot [3]★

[1]*Labortoire de Spectroscopie et Dynamique Moléculaire, LSDM, École Nationale Supérieure d'Ingénieurs de Tunis, University of Tunis, 1008, Tunisia*
[2]*Department of Physics, Common First Year Deanship, Umm Al-Qura University, 24382 Makkah al-Mukarramah, Saudi Arabia*
[3]*Observatoire de Paris, PSL University, Sorbonne Université, CNRS, LERMA, F-92190 Meudon, France*

Accepted 2022 February 10. Received 2022 January 23; in original form 2021 December 8

ABSTRACT

Missing Stark widths for 37 spectral lines of strontium ions (17 Sr V lines and 20 Sr VI lines) have been calculated using a quantum-mechanical method. Twenty-three spectral lines of Sr V have been recently discovered, for the first time, in the ultraviolet spectrum of the hot white dwarf RE 0503−289. This recent discovery prompts us to calculate the Stark widths of the new lines. These calculations can fill the lack of the data base STARK-B and can be used to investigate the observed spectra in such stars. To perform the line broadening calculations, preliminary structure and collision calculations have been carried out using the sequence of the University College London codes (SUPERSTRUCTURE, DISTORTED WAVE, and JAJOM). Results for the 37 lines are provided for different electron temperatures and at density $N_e = 10^{17}$ cm^{-3}. These results will enter the STARK-B data base, which is a node of the Virtual Atomic and Molecular Data Center. We hope that the obtained results will be useful for the non-local thermodynamic equilibrium modelling of stellar atmospheres.

Key words: atomic data – line: profiles – stars: atmospheres – stars: individual: RE 0503−289 – white dwarfs.

1 INTRODUCTION

Line broadening and atomic parameters of the emitters are necessary in the analysis and interpretation of the spectra recorded by spectrographs. Also, reliable measurements and calculations of these parameters are strongly needed for stellar atmosphere modelling. In Rauch et al. (2016a), the authors showed that the lack of structural and radiative atomic data of many elements is an obstacle to their abundance analysis, in particular for high ionization stages (IV–VII). Stark width data have solved many problems in the diagnostics of astrophysical plasma. Line widths of many elements are required to explore the stellar opacity and the radiative transfer (Dimitrijević 2003). Stark broadening is the main broadening mechanism of lines in different astrophysical conditions of density and temperature, especially for white dwarfs (WDs). Therefore, the lack of Stark broadening data can affect the accuracy of element abundance determination. Recently, Elabidi (2021) showed that the Stark broadening mechanism is dominant in hot WDs' atmospheres; Sahal-Bréchot & Elabidi (2021) showed that the Stark broadening mechanism is dominant in hot stars' atmospheres; Dimitrijević (2020) showed that the mechanism of Stark broadening is dominant in WDs of types A and B; and Aloui et al. (2019a) showed that the Stark broadening mechanism is dominant in hot helium-rich white dwarfs (spectral type DO). In the past, WDs were known as helium-rich (DB) and hydrogen-rich (DA) types. Nowadays, many papers (Rauch et al. 2017a,b, 2020; Werner et al. 2018a; Werner, Rauch & Kruk 2018b) have proved the existence of spectral lines emitted by several heavy elements in the UV spectra of hot WDs. Rauch et al. (2017b) mentioned that for the spectral analysis of high-resolution hot WDs, accurate results of atomic data are prerequisite for advanced non-local thermodynamic equilibrium (NLTE) stellar atmosphere modelling. These models should contain the opacity of heavy elements. In the meantime, 18 *trans*-iron elements with atomic numbers in the range $Z = 29$–56 were detected in the RE 0503−289 hot WD stars (Rauch et al. 2020). Recently, Rauch et al. (2017b) detected several heavy elements in hot WDs (Se V, Sr V, Te VI, and I VI). The inaccuracy or the lack of atomic and Stark broadening parameters represents a handicap for spectral analysis by means of NLTE model atmospheres (Rauch et al. 2007).

In our work, we concentrate on two ions: first, the Sr V ion, for which Rauch et al. (2017b) discovered 23 new lines in the UV spectrum of the hot WD RE 0503−289; secondly, the Sr VI ion that Persson & Pettersson (1984) and O'Sullian & Maher (1989) identified several lines for the first time. Rauch et al. (2017b) showed that the strongest Sr VI lines (identified by Persson & Pettersson 1984; O'Sullian & Maher 1989) are belonging to the extreme ultraviolet (EUV) and X-ray wavelength range of the DO WD RE 0503−289 spectrum. Spectra have been recorded with the *Far Ultraviolet Spectroscopic Explorer* (*FUSE*) and the *Hubble Space Telescope* (*HST*).

The aim of our work is to calculate the Stark widths of 17 Sr V lines (among the 23 new lines discovered by Rauch et al. 2017b) and the Stark widths of 20 Sr VI lines (among the strongest Sr VI lines identified by Persson & Pettersson 1984 and O'Sullian & Maher 1989). Along our calculations, atomic data (energy levels, line strengths, oscillator strengths, and spontaneous transition probabilities) for Sr V and Sr VI ions have been calculated using the University College London (UCL) codes [SUPERSTRUCTURE (SST) (Eissner, Jones & Nussbaumer 1974)/DISTORTED WAVE (DW) (Eissner 1998)/JAJOM (Saraph 1978)]. When comparisons are possible, we evaluate and compare the current atomic parameters used in the line-width calculations to ensure a good accuracy of the results. To perform the line broadening calculations, we have used our quantum-

★ E-mail: haelabidi@uqu.edu.sa (HE); rihab.aloui@ensit.u-tunis.tn (RA); sylvie.sahal-brechot@obspm.fr (SSB)

mechanical method (Elabidi, Ben Nessib & Sahal-Bréchot 2004; Elabidi et al. 2008). We applied this method many times (Aloui et al. 2018; Elabidi & Sahal-Bréchot 2019; Aloui, Elabidi & Sahal-Bréchot 2019b, 2020, 2021), and we found that it gives accurate results compared with other approaches that can be used with confidence in plasma diagnostics. The calculations have been performed at electron density $N_e = 10^{17}$ cm^{-3} and for electron temperatures between 10^4 and 5×10^5 K. Stark-width results for Sr VI and Sr VI are missing in the literature despite their importance for stellar plasma investigation. We hope that our calculations can fill the lack and enrich the data base STARK-B (Sahal-Bréchot, Dimitrijević & Moreau 2022). We introduce in Section 2 a brief description of our method and the numerical procedure used in the calculations. We provide our structure, radiative, and Stark broadening results and we discuss the validity conditions of the used approximations in Section 3. In Section 4, we investigate the influence of Stark broadening in the spectra of hot WDs. Finally, we conclude in Section 5.

2 BRIEF OVERVIEW OF THE LINE BROADENING METHOD

To calculate the electron Stark broadening of Sr V and Sr VI lines, we have used our quantum mechanical method (Elabidi et al. 2004, 2008). The full width at half-maximum (FWHM) W is

$$W = 2N_e \left(\frac{\hbar}{m}\right)^2 \left(\frac{2m\pi}{k_B T}\right)^{\frac{1}{2}} \times \int_0^\infty \Gamma_w(\epsilon) \exp\left(-\frac{\epsilon}{k_B T}\right) \mathrm{d}\left(\frac{\epsilon}{k_B T}\right), \quad (1)$$

where m denotes the electron mass, k_B denotes the Boltzmann constant, N_e denotes the electron density, T denotes the electron temperature, ϵ denotes the energy of the incident electron, and

$$\Gamma_w(\epsilon) = \sum_{J_i^T J_f^T l K_i K_f} \frac{\left[K_i, K_f, J_i^T, J_f^T\right]}{2} \times \begin{Bmatrix} J_i & K_i & l \\ K_f & J_f & 1 \end{Bmatrix}^2 \begin{Bmatrix} K_i & J_i^T & s \\ J_f^T & K_f & 1 \end{Bmatrix}^2 \times \left[1 - \left(\mathrm{Re}\left(\mathbf{S}_i\right)\mathrm{Re}\left(\mathbf{S}_f\right) + \mathrm{Im}\left(\mathbf{S}_i\right)\mathrm{Im}\left(\mathbf{S}_f\right)\right)\right], \quad (2)$$

where $L_i + \mathbf{S}_i = J_i$, $J_i + l = K_i$, and $K_i + s = J_i^T$. L and S are respectively the orbital and spin momenta of the target and l and s are those of the incident electron. The superscript T refers to the operators of the system (electron + target). $\mathbf{S}_i$ ($\mathbf{S}_f$) designates the scattering matrix elements for the initial (final) levels in intermediate coupling. Re (**S**) and Im (**S**) are the real and the imaginary parts of the **S** matrix, respectively. $\begin{Bmatrix} abc \\ def \end{Bmatrix}$ are the 6–j symbols and we use the notation $[x, y,...] = (2x + 1)(2y + 1)\ldots$. Re **S** and Im **S** are derived using the following expressions:

$$\mathrm{Re}\,\mathbf{S} = \left(1 - \mathbf{R}^2\right)\left(1 + \mathbf{R}^2\right)^{-1}, \mathrm{Im}\,\mathbf{S} = 2\mathbf{R}\left(1 + \mathbf{R}^2\right)^{-1}. \quad (3)$$

$\mathbf{S}_i$ and $\mathbf{S}_f$ are calculated at the same electron energy $\epsilon = mv^2/2$. The atomic data in intermediate coupling have been calculated by the SUPERSTRUCTURE (SST) code (Eissner et al. 1974), where configuration interaction and relativistic corrections (spin–orbit, mass, Darwin, and one-body) are taken into account according to the Breit–Pauli approach (Bethe & Salpeter 1957). The radial wave functions are determined by diagonalization of the non-relativistic Hamiltonian using orbitals calculated in a scaled Thomas–Fermi–Dirac–Amaldi (TFDA) potential. The potential depends on λ_l (scaling parameters), which are determined by a self-consistent energy minimization on the term energies used in our calculations. The electron–ion scattering calculations are performed by the DW code (Eissner 1998), producing reaction matrices **R** in Russell-Saunders (LS) coupling. The scattering calculations in intermediate coupling (IC) are treated by the JAJOM code (Saraph 1978). This code uses the term coupling coefficients (TCCs) – resulting from SST – and the **R** matrices in LS coupling (obtained by DW) to calculate collision strengths. JAJPOLARI is the transformed version of JAJOM (Elabidi & Dubau, unpublished results) that produces the reactance matrices **R** in intermediate coupling. The code RTOS (Dubau, unpublished results) calculates the scattering matrices **S** from the reactance matrices **R** and the real (Re**S**) and the imaginary (Im**S**) parts of the scattering matrices **S**, and arranges them as input suitable for formula (2). Feshbach resonances are included by means of the Gailitis formula (Gailitis 1963). We have extrapolated the factor $\Gamma_w(\epsilon)$ in formula (2), which contains the scattering matrix **S** below the threshold for the corresponding inelastic process. We have shown in Elabidi, Ben Nessib & Sahal-Bréchot (2009) that the inclusion of Feshbach resonances improves the agreement with experimental results, especially for low temperature.

3 RESULTS AND DISCUSSION

3.1 Structure and radiative data

We have used in SST (Eissner et al. 1974) five configurations for Sr V: $3d^{10}$ ($4s^24p^4$, $4s4p^5$, $4s^24p^34d$, $4s^24p^35s$, and $4s^24p^35p$). These configurations give us 85 fine structure levels and 43 LS terms. For Sr VI, we have used three configurations, $3d^{10}$ ($4s^24p^3$, $4s4p^4$, and $4s^24p^25s$), giving 21 fine structure levels and 11 LS terms. In Table 1, we display the present fine structure energy levels for Sr V in cm^{-1} and compare them with the National Institute of Standards and Technology (NIST) results (Kramida et al. 2021). The average error between our calculations and NIST results is less than 2 per cent. In Table 2, we display our fine structure energy levels for Sr VI in cm^{-1} and we compare them with the multiconfiguration Dirac–Fock (MCDF) results of Charro & Martín (1998) using the GRASP code developed by Grant et al. (1980) and Grant (1989), with the results of NIST (Kramida et al. 2021) and with the experimental results (Exp.) of Wyart & Artru (1989). We present also in Table 2 the average errors between our calculations and all the other results which are less than 4 per cent. Table 3 displays our transition probabilities A_{ij}, weighted oscillator strengths gf, and line strengths S for Sr V allowed transitions involving the ground and first excited levels. Table 4 displays our transition probabilities A_{ij} compared with the experimental results (Sansonetti 2012), weighted oscillator strengths gf compared with the MCDF results provided by O'Sullian (1989) using the MCDF code of Grant et al. (1980), and line strengths S for Sr VI allowed transitions involving the first five levels. The average error $\Delta_{\mathrm{Exp.}}$ between our calculations and the measurements for A_{ji} is ∼33 per cent, the transition $4s^24p^25s\ ^4P_{5/2}$–$4s^24p^3\ ^4S^o_{3/2}$ (16–1) presents the higher error. The average difference Δ_{MCDF} between our calculations and the MCDF results for gf is ∼30 per cent. The highest difference is found for the two transitions $4s^24p^25s\ ^4P_{5/2}$–$4s^24p^3\ ^4S^o_{3/2}$ (16–1) and $4s^24p^25s\ ^2D_{3/2}$–$4s^24p^3\ ^2D^o_{3/2}$ (20–2).

3.2 Line broadening results

3.2.1 Impact approximation

Before starting the calculations, we prove hereafter the validity of the impact approximation and the ideal plasma approximation for the plasma temperatures and density used in our work.

Table 1. Current Sr V fine structure energy levels (in cm^{-1}) compared with the NIST results (Kramida et al. 2021).

i	Level	Current	NIST	i	Level	Current	NIST
1	$4s^24p^4\ ^3P_2$	0.0	0.0	44	$4s^24p^3(^2D^o)4d\ ^3P^o$	288 382	275 425
2	$4s^24p^4\ ^3P_1$	8166	8308	45	$4s^24p^3(^4S^o)4d\ ^3D^o_1$	288 896	280 067
3	$4s^24p^4\ ^3P_0$	9085	8718	46	$4s^24p^3(^2D^o)5s\ ^3D^o_2$	291 049	289 117
4	$4s^24p^4\ ^1D_2$	23 172	20 311	47	$4s^24p^3(^2D^o)4d\ ^3P^o_1$	291 192	269 615
5	$4s^24p^4\ ^1S_0$	50 557	44 050	48	$4s^24p^3(^2D^o)5s\ ^3D^o_3$	293 001	291 836
6	$4s4p^5\ ^3P^o_2$	149 729	154 032	49	$4s^24p^3(^2D^o)5s\ ^3D^o_1$	293 148	288 832
7	$4s4p^5\ ^3P^o_1$	155 821	160 018	50	$4s^24p^3(^2D^o)4d\ ^1D^o_2$	295 986	285 450
8	$4s4p^5\ ^3P^o_0$	159 642	164 016	51	$4s^24p^3(^2D^o)5s\ ^1D^o_2$	297 391	294 818
9	$4s4p^5\ ^1P^o_1$	193 987	193 319	52	$4s^24p^3(^2D^o)4d\ ^1F^o_3$	306 945	291 678
10	$4s^24p^3(^4S^o)4d\ ^5D^o_0$	198 843	202 129	53	$4s^24p^3(^4S^o)5p\ ^5P_1$	309 307	313 726
11	$4s^24p^3(^4S^o)4d\ ^5D^o_1$	198 945	202 265	54	$4s^24p^3(^4S^o)5p\ ^5P_2$	309 903	314 143
12	$4s^24p^3(^4S^o)4d\ ^5D^o_2$	199 013	202 321	55	$4s^24p^3(^2P^o)5s\ ^3P^o_0$	310 602	306 607
13	$4s^24p^3(^4S^o)4d\ ^5D^o_3$	199 105	202 398	56	$4s^24p^3(^2P^o)5s\ ^3P^o_1$	311 375	307 806
14	$4s^24p^3(^4S^o)4d\ ^5D^o_4$	199 480	202 913	57	$4s^24p^3(^4S^o)5p\ ^5P_2$	311 623	314 143
15	$4s^24p^3(^2D^o)4d\ ^3F^o_2$	214 461	220 550	58	$4s^24p^3(^2P^o)5s\ ^3P^o_2$	314 583	311 700
16	$4s^24p^3(^2D^o)4d\ ^3D^o_3$	216 263	216 104	59	$4s^24p^3(^4S^o)5p\ ^3P_1$	317 927	319 835
17	$4s^24p^3(^2D^o)4d\ ^3D^o_1$	217 174	216 969	60	$4s^24p^3(^2P^o)5s\ ^1P^o_1$	318 290	314 736
18	$4s^24p^3(^2D^o)4d\ ^3D^o_2$	221 806	213 783	61	$4s^24p^3(^4S^o)5p\ ^3P_2$	318 878	321 239
19	$4s^24p^3(^2D^o)4d\ ^3F^o_3$	223 599	222 368	62	$4s^24p^3(^4S^o)5p\ ^3P_0$	319 423	321 641
20	$4s^24p^3(^2D^o)4d\ ^1S^o_0$	225 196	221 778	63	$4s^24p^3(^2P^o)4d\ ^1P^o_1$	323 767	306 075
21	$4s^24p^3(^2D^o)4d\ ^3F^o_4$	225 913	224 844	64	$4s^24p^3(^2D^o)5p\ ^3D_1$	331 597	331 198
22	$4s^24p^3(^2D^o)4d\ ^3G^o_3$	231 576	229 950	65	$4s^24p^3(^2D^o)5p\ ^3D_2$	334 606	336 695
23	$4s^24p^3(^2D^o)4d\ ^3G^o_4$	232 451	230 974	66	$4s^24p^3(^2D^o)5p\ ^3D_3$	336 666	339 930
24	$4s^24p^3(^2D^o)4d\ ^3G^o_5$	233 779	232 586	67	$4s^24p^3(^2D^o)5p\ ^3F_2$	337 041	334 365
25	$4s^24p^3(^2D^o)4d\ ^1G^o_4$	237 154	234 783	68	$4s^24p^3(^2D^o)5p\ ^1P_1$	337 627	337 454
26	$4s^24p^3(^2P^o)4d\ ^1D^o_2$	244 351	241 479	69	$4s^24p^3(^2D^o)5p\ ^1F_3$	339 092	338 692
27	$4s^24p^3(^2P^o)4d\ ^3D^o_1$	246 943	243 577	70	$4s^24p^3(^2D^o)5p\ ^3F_3$	340 168	336 623
28	$4s^24p^3(^2P^o)4d\ ^3P^o_0$	250 870	246 801	71	$4s^24p^3(^2D^o)5p\ ^3F_4$	340 333	340 419
29	$4s^24p^3(^2P^o)4d\ ^3D^o_2$	251 425	248 383	72	$4s^24p^3(^2D^o)5p\ ^3P_2$	347 431	343 583
30	$4s^24p^3(^2P^o)4d\ ^3P^o_1$	252 152	248 012	73	$4s^24p^3(^2D^o)5p\ ^3P_0$	347 977	345 057
31	$4s^24p^3(^2P^o)4d\ ^3F^o_3$	253 407	249 673	74	$4s^24p^3(^2D^o)5p\ ^3P_1$	348 012	345 344
32	$4s^24p^3(^2P^o)4d\ ^3F^o_2$	254 405	250 657	75	$4s^24p^3(^2P^o)5p\ ^3D_2$	354 666	356 567
33	$4s^24p^3(^2P^o)4d\ ^3F^o_4$	254 509	251 234	76	$4s^24p^3(^2P^o)5p\ ^1P_1$	356 251	363 332
34	$4s^24p^3(^2P^o)4d\ ^3D^o_3$	256 485	253 340	77	$4s^24p^3(^2P^o)5p\ ^3S_1$	358 639	357 248
35	$4s^24p^3(^2P^o)4d\ ^3P^o_2$	258 869	255 119	78	$4s^24p^3(^2D^o)5p\ ^1D_2$	358 808	351 337
36	$4s^24p^3(^4S^o)5s\ ^5S^o_2$	262 853	266 325	79	$4s^24p^3(^2P^o)5p\ ^3D_1$	361 113	353 845
37	$4s^24p^3(^2D^o)4d\ ^3S^o_1$	269 583	265 179	80	$4s^24p^3(^2P^o)5p\ ^3D_3$	361 155	359 647
38	$4s^24p^3(^2P^o)4d\ ^1F^o_3$	271 058	266 239	81	$4s^24p^3(^2P^o)5p\ ^3P_0$	362 393	358 076
39	$4s^24p^3(^4S^o)5s\ ^3S^o_1$	274 224	274 952	82	$4s^24p^3(^2P^o)5p\ ^3P_1$	365 646	357 554
40	$4s^24p^3(^2D^o)4d\ ^3P^o_2$	280 082	267 351	83	$4s^24p^3(^2P^o)5p\ ^1D_2$	367 023	362 487
41	$4s^24p^3(^4S^o)4d\ ^3D^o_3$	282 970	271 500	84	$4s^24p^3(^2P^o)5p\ ^3P_2$	367 172	364 887
42	$4s^24p^3(^2D^o)4d\ ^1P^o_1$	284 362	275 488	85	$4s^24p^3(^2P^o)5p\ ^1S_0$	382 131	375 152
43	$4s^24p^3(^4S^o)4d\ ^3D^o_2$	287 858	276 821				

The impact approximation states that the duration τ of an interaction must be much smaller than the mean interval time ΔT between two collisions (Baranger 1958):

$$\tau \ll \Delta T. \tag{4}$$

τ can be expressed as $\frac{\rho_{typ}}{v_{typ}}$, where ρ_{typ} is a typical impact parameter and v_{typ} is a mean typical velocity. ΔT is of the order of the inverse of the collisional line width, that is roughly equal to $N_e v_{typ} \rho^2_{typ}$. Consequently, we can write the validity condition of the impact approximation as

$$\rho_{typ} \ll N_e^{-1/3}. \tag{5}$$

ρ^3_{typ} is the 'collision volume', which must be smaller than the volume of one perturber N_e^{-1}. We can write the impact approximation condition in terms of the orbital momentum of the perturber and temperature. In fact, the classical angular momentum $\boldsymbol{L} = \rho m v$ can be related to the eigenvalues of the corresponding quantum-mechanical operator $\boldsymbol{L}^2$ by $\boldsymbol{L}^2 = (\rho m v)^2 = \hbar^2 l(l+1) \Longrightarrow \rho^2 = \frac{\hbar^2 l(l+1)}{(mv)^2}$, and using the expression of the velocity averaged over the Maxwell–Boltzmann distribution $v = \sqrt{\frac{8k_B T}{\pi m}}$ we find that a typical 'collision volume' can be written as (with $T_{typ} = 5 \times 10^5$ K and $l_{typ} = 29$)

$$\rho_{typ} = \left(\frac{\pi l^2_{typ} \hbar^2}{8 m k_B T_{typ}} \right)^{1/2} = 7.65 \times 10^{-8} \text{cm}. \tag{6}$$

With $N_e = 10^{17}$ cm^{-3}, we find $\rho_{typ} \ll N_e^{-1/3} = 2.14 \times 10^{-6}$ cm.

3.2.2 *Approximation of ideal plasma*

In order to prove that the criterion of plasma ideality is valid for the density and electron temperatures chosen in our work, it must be shown that the number of particles (perturbers) N_D inside the Debye sphere of radius R_D (the distance over which electric charges screen out the electric fields) is greater than 1. This can be written as

Table 2. Current Sr VI fine structure energy levels (in cm^{-1}) compared with the MCDF results (Charro & Martín 1998) using the GRASP code developed by Grant et al. (1980) and Grant (1989), with the NIST results (Kramida et al. 2021) and with the experimental results (Exp.) of Wyart & Artru (1989). Δ_X represents the relative error between our calculations and the results of X.

i	Level	Present	MCDF	NIST	Exp.	Δ_{MCDF}	Δ_{NIST}	Δ_{Exp}
1	$4s^24p^3\ ^4S^o_{3/2}$	0.0	0.0	0.0	–	–	–	–
2	$4s^24p^3\ ^2D^o_{3/2}$	24 653	24 803	20 135	–	1	18	–
3	$4s^24p^3\ ^2D^o_{5/2}$	27 508	28 684	23 527	–	4	14	–
4	$4s^24p^3\ ^2P^o_{1/2}$	45 048	40 809	38 531	–	10	14	–
5	$4s^24p^3\ ^2P^o_{3/2}$	49 123	46 013	43 567	–	7	11	–
6	$4s4p^4\ ^4P_{5/2}$	158 470	–	153 171	–	–	3	–
7	$4s4p^4\ ^4P_{3/2}$	164 772	–	159 597	–	–	3	–
8	$4s4p^4\ ^4P_{1/2}$	167 575	–	162 238	–	–	3	–
9	$4s4p^4\ ^2D_{3/2}$	212 487	–	188 319	–	–	11	–
10	$4s4p^4\ ^2D_{5/2}$	213 319	–	189 978	–	–	11	–
11	$4s4p^4\ ^2S_{1/2}$	238 724	–	227 292	–	–	5	–
12	$4s4p^4\ ^2P_{3/2}$	258 959	–	215 697	–	–	17	–
13	$4s4p^4\ ^2P_{1/2}$	266 993	–	216 644	–	–	19	–
14	$4s^24p^25s\ ^4P_{1/2}$	331 030	328 485	327 320	327 472	1	1	1
15	$4s^24p^25s\ ^4P_{3/2}$	335 906	334 076	333 260	333 414	1	1	1
16	$4s^24p^25s\ ^4P_{5/2}$	341 062	337 474	338 650	338 739	1	1	1
17	$4s^24p^25s\ ^2P_{1/2}$	343 329	341 072	338 240	338 399	1	1	1
18	$4s^24p^25s\ ^2P_{3/2}$	348 889	347 223	343 870	343 976	0	1	1
19	$4s^24p^25s\ ^2D_{5/2}$	360 937	360 449	355 820	355 890	0	1	1
20	$4s^24p^25s\ ^2D_{3/2}$	361 875	361 481	356 820	356 928	0	1	1
21	$4s^24p^25s\ ^2S_{1/2}$	387 831	388 487	378 990	379 200	0	2	2

Table 3. Current spontaneous transition probabilities A_{ij}, weighted oscillator strengths *gf*, and line strengths *S* for Sr V allowed transitions. *i* and *j* label the levels of Table 1. We present only ten rows, and the remaining data are included in the supplementary material.

i–j	A_{ij} (s^{-1})	*gf*	*S*	*i–j*	A_{ij} (s^{-1})	*gf*	*S*
6–1	9.670E+08	3.233E−01	0.710 93	6–2	3.087E+08	1.155E−01	0.268 55
7–1	6.419E+08	1.189E−01	0.251 21	7–2	3.244E+08	6.693E−02	0.149 23
9–1	9.627E+07	1.151E−02	0.019 53	8–2	1.356E+09	8.863E−02	0.192 62
11–1	5.427E+07	6.168E−03	0.010 21	9–2	8.862E+06	1.154E−03	0.002 05
12–1	6.535E+07	1.237E−02	0.020 46	10–2	8.012E+07	3.304E−03	0.005 70
13–1	3.129E+07	8.282E−03	0.013 70	11–2	2.802E+07	3.462E−03	0.005 98
15–1	1.472E+08	2.399E−02	0.036 83	12–2	2.177E+05	4.481E−05	0.000 08
16–1	9.960E+07	2.235E−02	0.034 02	15–2	4.570E+07	8.050E−03	0.012 85
17–1	3.735E+07	3.562E−03	0.005 40	17–2	1.297E+08	1.335E−02	0.021 04
18–1	5.029E+07	7.663E−03	0.011 37	18–2	2.148E+07	3.527E−03	0.005 44

Table 4. Current spontaneous transition probabilities A_{ij} compared with the experimental results (Exp.) of Sansonetti (2012), weighted oscillator strengths *gf* compared with the MCDF results of O'Sullian (1989) using the MCDF code of Grant et al. (1980), and line strengths *S* for Sr VI allowed transitions. *i* and *j* label the levels of Table 2. Δ_X represents the relative error between our calculations and the results of X. We present only ten rows, and the remaining data are included in the supplementary material.

Levels	$A_{ij}(s^{-1})$			*gf*			*S*
i–j	Current	Exp.	$\Delta_{Exp.}$ (per cent)	Current	MCDF	Δ_{MCDF} (per cent)	
6–1	4.657E+09	–	–	1.668E+00	–	–	3.465 267
7–1	5.286E+09	–	–	1.168E+00	–	–	2.332 652
8–1	5.631E+09	–	–	6.013E−01	–	–	1.181 254
9–1	6.536E+07	–	–	8.681E−03	–	–	0.013 450
11–1	8.108E+07	–	–	4.266E−03	–	–	0.005 883
12–1	6.046E+08	–	–	5.406E−02	–	–	0.068 732
13–1	4.594E+07	–	–	1.933E−03	–	–	0.002 383
14–1	1.089E+10	6.000E+09	45	2.981E−01	1.670E−01	44	0.296 414
15–1	1.086E+10	8.500E+09	22	5.772E−01	3.050E−01	47	0.565 687
16–1	1.112E+10	5.500E+09	51	8.596E−01	4.320E−01	50	0.829 764

Table 5. Our quantum full Stark widths W for 17 Sr V lines at electron density $N_e = 10^{17}$ cm^{-3} for different temperatures. The wavelengths λ are taken from the SST code (Eissner et al. 1974).

Transition	T (10^4 K)	W (pm)	Transition	W (pm)
	1	1.141E+01		1.186E+01
$4p^3(^2P^o)4d\ ^3D^o_3$–$4p^3(^2P^o)5p\ ^1D_2$	2	7.703E+00	$4p^3(^2D^o)4d\ ^3D^o_2$–$4p^3(^4S^o)5p\ ^3P_1$	8.024E+00
λ = 904.67 Å	4	4.604E+00	λ = 1040.35 Å	4.915E+00
	6	3.515E+00		3.863E+00
	8	2.950E+00		3.331E+00
	10	2.585E+00		2.996E+00
	1	9.015E+00		1.982E+01
$4p^3(^2D^o)4d\ ^3G^o_4$–$4p^3(^2D^o)5p\ ^3F_3$	2	6.019E+00	$4p^3(^2P^o)4d\ ^1F^o_3$–$4p^3(^2P^o)5p\ ^3P_2$	1.143E+01
λ = 928.36 Å	4	3.486E+00	λ = 1040.43 Å	6.254E+00
	6	2.586E+00		4.644E+00
	8	2.127E+00		3.841E+00
	10	1.839E+00		3.336E+00
	1	1.444E+01		5.891E+01
$4p^3(^2P^o)4d\ ^3F^o_4$–$4p^3(^2P^o)5p\ ^3D_3$	2	8.620E+00	$4p^3(^2P^o)4d\ ^1F^o_3$–$4p^3(^2P^o)5p\ ^1D_2$	2.432E+01
λ = 937.68 Å	4	4.673E+00	λ = 1042.05 Å	9.569E+00
	6	3.391E+00		5.847E+00
	8	2.742E+00		4.340E+00
	10	2.333E+00		3.546E+00
	1	3.705E+01		1.776E+01
$4p^3(^2P^o)4d\ ^3P^o_1$–$4p^3(^2P^o)5p\ ^3S_1$	2	1.801E+01	$4p^3(^2P^o)4d\ ^1D^o_2$–$4p^3(^2D^o)5p\ ^1P_1$	1.149E+01
λ = 939.08 Å	4	9.019E+00	λ = 1072.09 Å	6.668E+00
	6	6.476E+00		5.040E+00
	8	5.248E+00		4.224E+00
	10	4.495E+00		3.719E+00
	1	7.893E+00		2.294E+01
$4p^3(^2D^o)4d\ ^3D^o_3$–$4p^3(^4S^o)5p\ ^3P_2$	2	5.329E+00	$4p^3(^2P^o)4d\ ^3D^o_2$–$4p^3(^2D^o)5p\ ^3F_2$	1.463E+01
λ = 974.52 Å	4	3.219E+00	λ = 1168.01 Å	8.543E+00
	6	2.500E+00		6.511E+00
	8	2.143E+00		5.458E+00
	10	1.925E+00		4.777E+00
	1	8.362E+00		2.018E+01
$4p^3(^2D^o)4d\ ^1G^o_4$–$4p^3(^2D^o)5p\ ^1F_3$	2	5.425E+00	$4p^3(^2P^o)4d\ ^3D^o_1$–$4p^3(^2D^o)5p\ ^3D_1$	1.650E+01
λ = 980.98 Å	4	3.135E+00	λ = 1181.28 Å	1.121E+01
	6	2.359E+00		8.688E+00
	8	1.969E+00		7.267E+00
	10	1.726E+00		6.343E+00
	1	2.408E+01		3.215E+01
$4p^3(^2P^o)4d\ ^3F^o_3$–$4p^3(^2P^o)5p\ ^3D_2$	2	1.239E+01	$4p^3(^2P^o)4d\ ^3D^o_2$–$4p^3(^4S^o)5p\ ^3P_2$	1.878E+01
λ = 987.58 Å	4	6.262E+00	λ = 1482.52 Å	1.118E+01
	6	4.449E+00		8.891E+00
	8	3.570E+00		7.655E+00
	10	3.037E+00		6.822E+00
	1	5.022E+01		2.992E+01
$4p^3(^2P^o)4d\ ^3D^o_1$–$4p^3(^2D^o)5p\ ^3P_0$	2	2.132E+01	$4p^3(^2D^o)4d\ ^3P^o_2$–$4p^3(^2D^o)5p\ ^3D_3$	1.796E+01
λ = 989.77 Å	4	9.999E+00	λ = 1767.26 Å	1.189E+01
	6	7.078E+00		1.032E+01
	8	5.735E+00		9.444E+00
	10	4.937E+00		8.780E+00
	1	7.568E+00		
$4p^3(^2D^o)4d\ ^1G^o_4$–$4p^3(^2D^o)5p\ ^3D_3$	2	5.448E+00		
λ = 1004.90 Å	4	3.367E+00		
	6	2.581E+00		
	8	2.174E+00		
	10	1.919E+00		

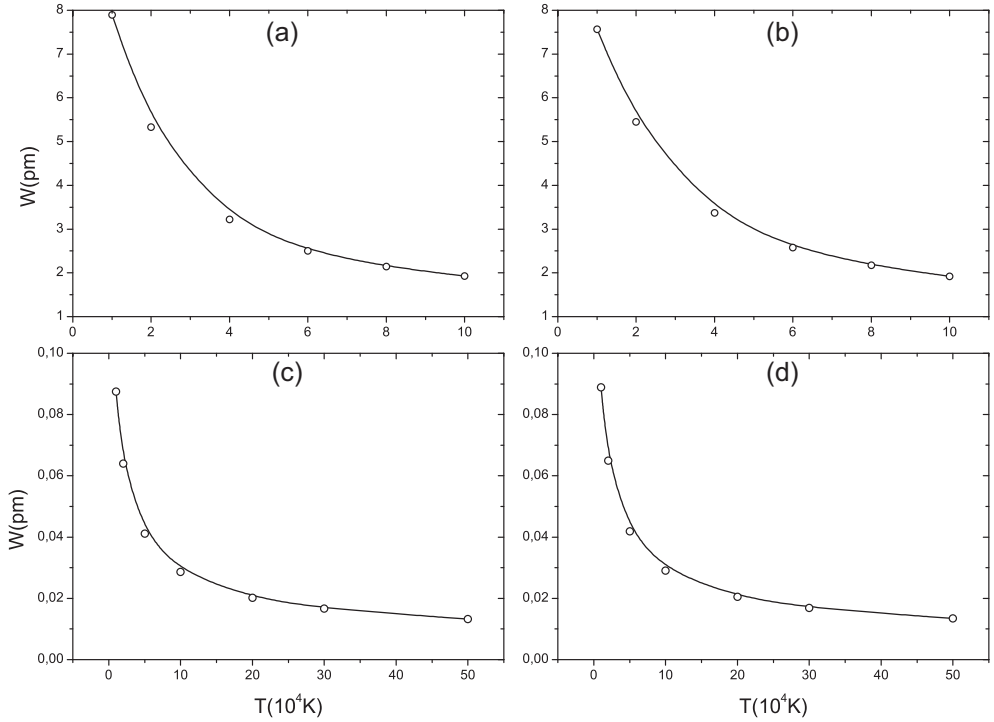

Figure 1. Stark broadening as a function of electron temperature for the two Sr V transitions, $4p^3(^2D^o)4d\ ^3D^o_3$–$4p^3(^4S^o)5p\ ^3P_2$ (16–61) (a) and $4p^3(^2D^o)4d\ ^1G^o_4$–$4p^3(^2D^o)5p\ ^3D_3$ (25–66) (b), and for the two Sr VI transitions, $4s^24p^25s\ ^2S_{1/2}$–$4s^24p^3\ ^2P^o_{1/2}$ (21–4) (c) and $4s^24p^25s\ ^2S_{1/2}$–$4s^24p^3\ ^2P^o_{3/2}$ (21–5) (d). Electron density $N_e = 10^{17}$ cm^{-3}.

(Dimitrijević, Sahal-Bréchot & Bommier 1991)

$$N_D = N_e V > 1, \tag{7}$$

where $V = \frac{4\pi}{3} R_D^3$ is the volume of the Debye sphere. R_D is the Debye length (or Debye radius), which can be written as

$$R_D = \sqrt{\frac{\varepsilon_0 k_B T}{N_e e^2}}, \tag{8}$$

where ε_0 is the permittivity of free space and e is the elementary charge in SI units. We can write the inequality (7) as

$$N_e > \frac{3}{4\pi R_D^3}, \tag{9}$$

$$N_e < \left(\frac{4\pi}{3}\right)^2 \left(\frac{\varepsilon_0 k_B}{e^2}\right)^3 T^3. \tag{10}$$

So, the condition of the plasma ideality can be written by the following inequality:

$$N_e(\mathrm{cm}^{-3}) < 1.9 \times 10^6 T^3\,(\mathrm{K}). \tag{11}$$

In WD atmospheres, the plasma becomes non-ideal with the decrease of temperature or increase of density. As an example, if we take the lowest temperature used in our work $T = 10^4$ K, we find that $N_e < 1.9 \times 10^{18}$ cm^{-3}. If we take the highest temperature $T = 5 \times 10^5$ K, we find that $N_e < 2.38 \times 10^{23}$ cm^{-3}. So, our plasma is ideal for the considered density $N_e = 10^{17}$ cm^{-3} and temperatures. Therefore, we can deduce the Stark line widths for other densities using a linear relationship between W and N_e (for a given temperature) provided that these densities are lower than 10^{23} cm^{-3}, at which the plasma can be considered as ideal.

3.2.3 *Stark broadening results for Sr V*

In Table 5, we display the Stark broadening of 17 Sr V lines. The calculations are performed at electron density $N_e = 10^{17}$ cm^{-3} and for electron temperatures ranging from 10^4 to 10^5 K using five configurations for the Sr V structure. There are two Sr V lines described as 'uncertain' (915.994 and 985.408 Å) and four Sr V lines (935.509, 951.044, 962.378, and 1379.615 Å) described as 'blend' (blended with lines of other species) in the UV spectrum of RE 0503−289 (Rauch et al. 2017b). The 'uncertain' and 'blend' lines are considered in Table 5 because they are identified in the NIST data base (Kramida et al. 2021) and in Sansonetti (2012). We found that the Sr V lines are given in the NIST data base with the corresponding initial and final levels and their wavelengths. In order to illustrate the behaviour of the Stark broadening with temperature, we display in Fig. 1 our line widths as a function of electron temperature and at electron density $N_e = 10^{17}$ cm^{-3} for the two Sr V transitions: $4p^3(^2D^o)4d\ ^3D^o_3$–$4p^3(^4S^o)5p\ ^3P_2$ (16–61) (panel a) and $4p^3(^2D^o)4d\ ^1G^o_4$–$4p^3(^2D^o)5p\ ^3D_3$ (25–66) (panel b).

3.2.4 *Stark broadening results for Sr VI*

In Table 6, we display the Stark broadening of the 20 strongest lines of Sr VI. The calculations are performed at electron density $N_e = 10^{17}$ cm^{-3} and for electron temperatures ranging from 10^4 to 5×10^5 K required for plasma modelling. Three configurations have been used for the Sr VI structure calculation. Nine of these lines were identified for the first time by Persson & Pettersson (1984), who identified all the levels corresponding to the ground configuration ($4s^24p^3$) and the first excited configuration ($4s4p^4$). The other 11 lines were identified for the first time by O'Sullian & Maher (1989). In order to illustrate the behaviour of the Stark broadening with

Table 6. Same as Table 5 but for 20 Sr VI lines.

Transition	T (10^4 K)	W (pm)	Transition	W (pm)
	1	8.747E−02		1.065E−01
$4s^24p^25s\ ^2S_{1/2}$–$4s^24p^3\ ^2P^o_{1/2}$	2	6.396E−02	$4s^24p^25s\ ^2P_{3/2}$–$4s^24p^3\ ^2P^o_{3/2}$	7.724E−02
$\lambda = 291.73$ Å	5	4.118E−02	$\lambda = 333.59$ Å	4.986E−02
	10	2.860E−02		3.472E−02
	20	2.019E−02		2.452E−02
	30	1.666E−02		2.023E−02
	50	1.320E−02		1.606E−02
	1	8.005E−02		3.023E−01
$4s^24p^25s\ ^4P_{5/2}$–$4s^24p^3\ ^4S^o_{3/2}$	2	5.795E−02	$4s4p^4\ ^2P_{1/2}$–$4s^24p^3\ ^2D^o_{3/2}$	1.800E−01
$\lambda = 293.20$ Å	5	3.747E−02	$\lambda = 412.64$ Å	8.608E−02
	10	2.613E−02		5.739E−02
	20	1.844E−02		4.143E−02
	30	1.518E−02		3.494E−02
	50	1.197E−02		2.862E−02
	1	8.887E−02		3.313E−01
$4s^24p^25s\ ^2S_{1/2}$–$4s^24p^3\ ^2P^o_{3/2}$	2	6.499E−02	$4s4p^4\ ^2P_{3/2}$ –$4s^24p^3\ ^2D^o_{5/2}$	1.974E−01
$\lambda = 295.24$ Å	5	4.184E−02	$\lambda = 432.06$ Å	9.449E−02
	10	2.905E−02		6.301E−02
	20	2.052E−02		4.545E−02
	30	1.693E−02		3.832E−02
	50	1.342E−02		3.142E−02
	1	8.084E−02		1.178E−01
$4s^24p^25s\ ^2D_{3/2}$–$4s^24p^3\ ^2D^o_{3/2}$	2	5.827E−02	$4s4p^4\ ^2S_{1/2}$–$4s^24p^3\ ^2P^o_{1/2}$	9.987E−02
$\lambda = 296.54$ Å	5	3.776E−02	$\lambda = 516.32$ Å	8.521E−02
	10	2.644E−02		6.916E−02
	20	1.871E−02		5.440E−02
	30	1.544E−02		4.709E−02
	50	1.225E−02		3.930E−02
	1	8.133E−02		1.040E−01
$4s^24p^25s\ ^2D_{5/2}$–$4s^24p^3\ ^2D^o_{3/2}$	2	5.846E−02	$4s4p^4\ ^2D_{3/2}$–$4s^24p^3\ ^2D^o_{3/2}$	7.619E−02
$\lambda = 297.37$ Å	5	3.765E−02	$\lambda = 532.39$ Å	5.580E−02
	10	2.625E−02		4.972E−02
	20	1.853E−02		4.442E−02
	30	1.527E−02		4.068E−02
	50	1.210E−02		3.567E−02
	1	8.269E−02		1.048E−01
$4s^24p^25s\ ^4P_{3/2}$–$4s^24p^3\ ^4S^o_{3/2}$	2	5.985E−02	$4s4p^4\ ^2D_{5/2}$–$4s^24p^3\ ^2D^o_{5/2}$	7.662E−02
$\lambda = 297.70$ Å	5	3.868E−02	$\lambda = 538.18$ Å	5.615E−02
	10	2.696E−02		5.016E−02
	20	1.901E−02		4.482E−02
	30	1.565E−02		4.102E−02
	50	1.234E−02		3.594E−02
	1	8.256E−02		8.626E−02
$4s^24p^25s\ ^2D_{5/2}$–$4s^24p^3\ ^2D^o_{5/2}$	2	5.948E−02	$4s4p^4\ ^4P_{1/2}$–$4s^24p^3\ ^4S^o_{3/2}$	6.264E−02
$\lambda = 299.91$ Å	5	3.850E−02	$\lambda = 596.75$ Å	4.808E−02
	10	2.694E−02		4.683E−02
	20	1.905E−02		4.442E−02
	30	1.572E−02		4.143E−02
	50	1.246E−02		3.673E−02
	1	8.564E−02		8.474E−02
$4s^24p^25s\ ^4P_{1/2}$–$4s^24p^3\ ^4S^o_{3/2}$	2	6.188E−02	$4s4p^4\ ^4P_{3/2}$–$4s^24p^3\ ^4S^o_{3/2}$	6.158E−02
$\lambda = 302.09$ Å	5	4.001E−02	$\lambda = 606.90$ Å	4.780E−02
	10	2.791E−02		4.732E−02
	20	1.970E−02		4.535E−02
	30	1.621E−02		4.245E−02
	50	1.279E−02		3.773E−02
	1	8.719E−02		1.337E−01
$4s^24p^25s\ ^2P_{3/2}$–$4s^24p^3\ ^2D^o_{5/2}$	2	6.294E−02	$4s4p^4\ ^2D_{5/2}$–$4s^24p^3\ ^2P^o_{3/2}$	9.880E−02
$\lambda = 311.16$ Å	5	4.083E−02	$\lambda = 609.03$ Å	7.392E−02

Table 6 – *continued*

Transition	T (10^4 K)	W (pm)	Transition	W (pm)
	10	2.860E−02		6.700E−02
	20	2.025E−02		5.978E−02
	30	1.673E−02		5.449E−02
	50	1.330E−02		4.750E−02
	1	9.945E−02		9.040E−02
$4s^24p^25s\ ^2D_{3/2}$–$4s^24p^3\ ^2P^o_{3/2}$	2	7.211E−02	$4s4p^4\ ^4P_{5/2}$–$4s^24p^3\ ^4S^o_{3/2}$	6.572E−02
$\lambda = 319.74$ Å	5	4.658E−02	$\lambda = 631.04$ Å	5.116E−02
	10	3.246E−02		5.081E−02
	20	2.294E−02		4.882E−02
	30	1.892E−02		4.573E−02
	50	1.501E−02		4.068E−02

Table 7. Our quantum Stark widths W and the results of the Cowley formula W_C (Cowley 1971) expressed in picometres for Sr V lines at two electron temperatures and at electron density $N = 10^{17}$ cm^{-3}. The temperature T is expressed in 10^4 K and $R = W_C/W$.

Line	T	W	W_C	R
$4p^3(^2D^o)4d\ ^3G^o_4$–$4p^3(^2D^o)5p\ ^3F_3$	1	9.015	18.85	2.09
$\lambda = 928.36$ Å	4	3.486	18.85	5.41
$4p^3(^2P^o)4d\ ^3F^o_4$–$4p^3(^2P^o)5p\ ^3D_3$	1	14.44	23.29	1.61
$\lambda = 937.68$ Å	4	4.673	23.29	4.98
$4p^3(^2P^o)4d\ ^3P^o_1$–$4p^3(^2P^o)5p\ ^3S_1$	1	37.05	19.29	0.52
$\lambda = 939.08$ Å	4	9.019	19.29	2.14
$4p^3(^2D^o)4d\ ^3D^o_3$–$4p^3(^4S^o)5p\ ^3P_2$	1	7.893	17.40	2.20
$\lambda = 974.52$ Å	4	3.219	17.40	5.41
$4p^3(^2D^o)4d\ ^1G^o_4$–$4p^3(^2D^o)5p\ ^1F_3$	1	8.362	20.85	2.49
$\lambda = 980.98$ Å	4	3.135	20.85	6.65

temperature, we display in Fig. 1 our line widths as a function of electron temperature and at electron density $N_e = 10^{17}$ cm^{-3} for the two Sr VI transitions: $4s^24p^25s\ ^2S_{1/2}$–$4s^24p^3\ ^2P^o_{1/2}$ (21–4) (panel c) and $4s^24p^25s\ ^2S_{1/2}$–$4s^24p^3\ ^2P^o_{3/2}$ (21–5) (panel d). We could not find other results in the literature to compare with the present Sr V and Sr VI Stark width data. The acceptable agreement found between our atomic data and other ones shows that the current line width results have an acceptable accuracy and can be used with trust in plasma investigations. Other experimental results or calculations of Sr V–VI broadening would be very helpful to confirm our calculations. Results of line widths in Tables 5 and 6 will be implemented in the STARK-B data base (available at http://stark-b.obspm.fr; Sahal-Bréchot, Dimitrijević & Moreau 2020; see also Roueff et al. 2020). STARK-B is free access and contains widths and shifts of isolated lines of ions and neutral atoms, perturbed by electron and ions for various temperatures and electron and ion densities. It is devoted to modelling and spectroscopic diagnostics of stellar atmospheres and envelopes and laboratory, fusion, and technological plasmas. It is a node of the Virtual Atomic and Molecular Data Center (VAMDC Consortium: http://www.vamdc.eu/) (Albert et al. 2020).

3.2.5 Comparison with the Cowley approximate formula

We calculate Stark widths for five Sr V lines using the Cowley approximate formula (Cowley 1971) in order to compare them with our quantum results and illustrate the difference between our rigorous calculations and the approximation. The approximate formula is proposed for one electron temperature $T = 10^4$ K, and Cowley (1971) mentioned that the formula is not recommended when detailed calculations or experimental results are available. We use it here to show that it overestimates the Stark broadening, as mentioned in Dimitrijević et al. (2005). The Stark broadening W_C, expressed in angstroms, is calculated by the formula (Cowley 1971)

$$W_C = 2 \times 0.77 \times 10^{-18} (n^*)^4 \lambda^2 N, \tag{12}$$

where N is the electron density in cm^{-3}, λ is the wavelength of the considered transition in centimetres, and n^* is the effective principal quantum number of the upper level defined by

$$n^* = Z \left(\frac{13.59}{I - E} \right)^{1/2}. \tag{13}$$

In equation (13), Z is the charge seen by the active electron ($Z = 1$ for neutral atoms,. . .), E is the energy of the level, and I is the appropriate series limit. Table 7 displays our quantum Stark broadening data for some Sr V lines compared with those calculated using the Cowley approximate formula (Cowley 1971) at two electron temperature values. The electron density is $N = 10^{17}$ cm^{-3}. We recall that formula (12) is proposed for one electron temperature $T = 10^4$ K, so the Stark broadening values W_C in Table 7 are the same for any chosen temperature.

We can see from Table 7 that in almost all the cases the approximate formula gives line widths that are greater than ours. Secondly, even at the electron temperature of $T = 10^4$ K, for which the formula is proposed, the two results disagree for almost all the lines and the ratio W_C/W varies between 0.52 and 2.49. For the electron temperature $T = 4 \times 10^4$ K, the disagreement between the two results becomes higher and the ratio W_C/W can reach 6.65. We can predict that for other temperatures further away from $T = 10^4$ K, the agreement will be worse. Consequently, while the approximate formula (12) is very easy to use, it is not recommended when measurements or rigorous calculations can be performed.

4 INFLUENCE OF STARK BROADENING IN THE SPECTRA OF HOT WHITE DWARFS

In order to prove the importance of our Stark broadening calculations, it is essential to explore the usefulness of the Stark broadening mechanism in the atmosphere of the considered star. To perform this task, we have compared the effect of Stark and Doppler broadening in many atmospheric layers and for different stellar atmospheres. We have used the model atmospheres of Wesemael (1981). The expression of Doppler broadening is

$$W_{\rm Doppler} = \lambda_0 \left(\frac{2 k_B T}{M c^2} \right)^{\frac{1}{2}}, \tag{14}$$

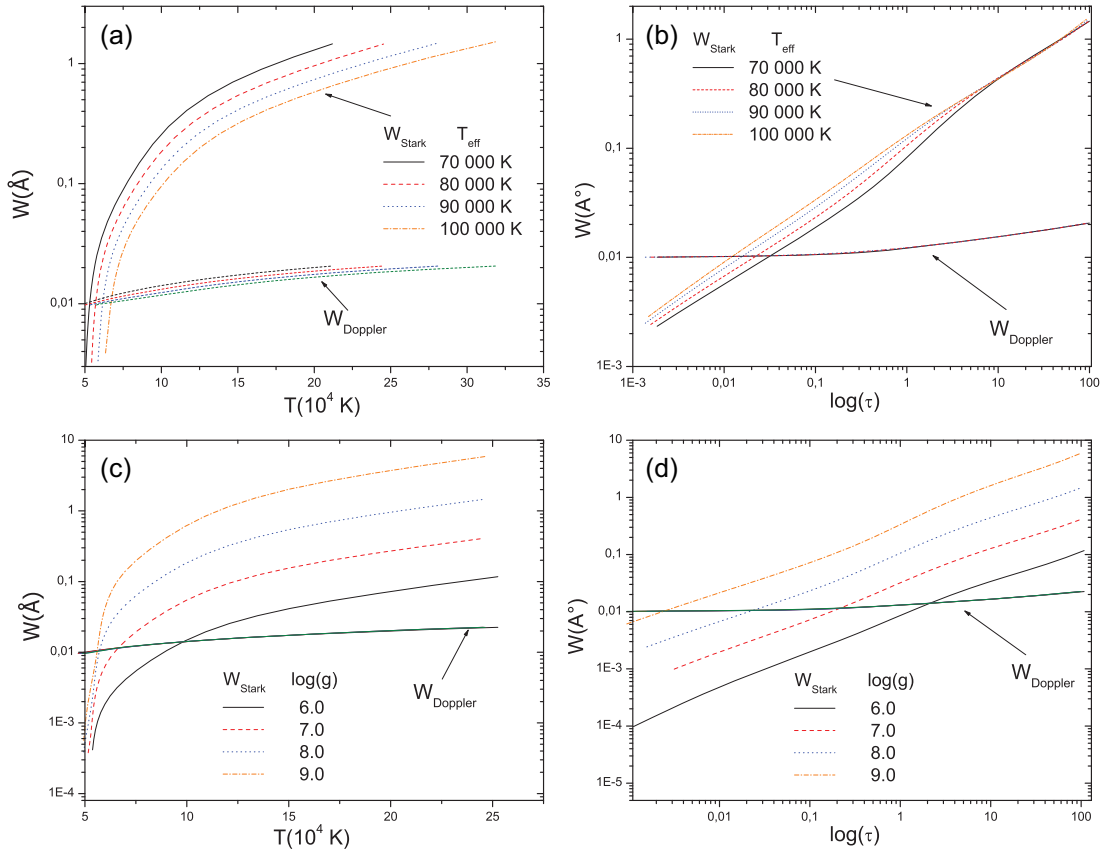

Figure 2. Stark $W_{\rm Stark}$ and Doppler $W_{\rm Doppler}$ widths for Sr V line $4p^3(^2D^o)4d\ ^3D^o_3$–$4p^3(^4S^o)5p\ ^3P_2$ ($\lambda = 974.52$ Å) for the atmospheric models of Wesemael (1981) with effective temperatures $T_{\rm eff} = 70\,000$–$100\,000$ K and $\log g = 8$ as a function of atmospheric layer temperatures (a) and as a function of the Rosseland optical depth (b), and for the atmospheric models of Wesemael (1981) with $\log g = 6$–9 and effective temperature $T_{\rm eff} = 80\,000$ K as a function of atmospheric layer temperatures (c) and as a function of the Rosseland optical depth (d).

where M denotes the atomic mass of the radiating atom (Sr) and c denotes the speed of light in vacuum expressed in the SI system. When we calculated the Stark and Doppler broadening, we found that their behaviours are the same for all the chosen lines. Consequently, we chose for illustration the Sr V line $4p^3(^2D^o)4d\ ^3D^o_3$–$4p^3(^4S^o)5p\ ^3P_2$ ($\lambda = 974.52$ Å).

We display the Stark and Doppler broadening for the Sr V line ($\lambda = 974.52$ Å) as a function of atmospheric layer temperatures (Fig. 2a) and as a function of the Rosseland optical depth (Fig. 2b) for atmospheric models with effective temperatures $T_{\rm eff} = 70\,000$–$100\,000$ K and $\log g = 8$ (Wesemael 1981). For $T > 70\,000$ K, the Stark width becomes more dominant than the Doppler width for all the atmospheric layer temperatures. We notice that the dominance is higher at deeper atmospheric layers. We come to the same conclusion if we examine the Stark and Doppler broadening as a function of the Rosseland optical depth in logarithmic scale ($\log \tau$) for the same atmospheric models (Fig. 2b): We notice that the Stark broadening is more significant relative to the Doppler broadening even at the surface of the DO WD atmospheres. Also, the Stark and Doppler broadening behaviours have been investigated as a function of atmospheric layer temperatures (Fig. 2c) and as a function of the Rosseland optical depth (Fig. 2d) for atmospheric models (Wesemael 1981) with $\log g = 6$–9 and $T_{\rm eff} = 80\,000$ K. For a gravity surface $\log g = 7$–9, the Stark line width becomes significant for temperatures of $\sim 10^5$ K (Fig. 2c). For $\log g = 6$, the Doppler width is more significant than the Stark width for lower temperatures (5×10^4 to 10^5 K), but for $T > 10^5$ K, the Stark width starts to dominate the Doppler width. For $\log g = 9$, we find that $W_{\rm Stark} \approx 2 \times W_{\rm Doppler}$ for the deepest atmospheric layer $T = 2.5 \times 10^5$ K. Concerning the variation of Stark and Doppler line widths with the Rosseland optical depth, Stark broadening is most significant for all the optical depths for the four atmospheric models $\log g = 6$–9 and is nearly more than twice the Doppler one for $\log g = 9$. We can conclude that Stark broadening is dominant compared with the Doppler broadening for all the atmospheric models of these DO WD atmospheres.

5 SUMMARY

We have calculated the Stark widths of 37 strontium lines (17 Sr V lines and 20 Sr VI lines) using our quantum-mechanical method. All the Stark widths are the first to be published. The calculations and comparisons of the intermediate results (energy levels and radiative atomic data) allow us to have an idea about the accuracy of our line-width calculations, since they are used in the calculations of line broadening. The obtained results will be of importance for the spectral analysis by means of NLTE model atmospheres. The results are provided for the range of temperatures from 10^4 to 5×10^5 K suitable for many astrophysical investigations, and at electron density $N_{\rm e} = 10^{17}$ cm^{-3}. The idea behind our work was the recent discovery of 23 new Sr V lines in the UV spectrum of the hot WD RE 0503−289 (Rauch et al. 2017b). Thus, we have calculated the Stark broadening for 17 Sr V lines – among the 23 new Sr V lines in Rauch et al. (2017b)

– and for the 20 strongest lines of Sr VI, which were identified, for the first time, by Persson & Pettersson (1984) and O'Sullian & Maher (1989).

Finally, we have investigated the importance of the Stark broadening $W_{\rm Stark}$ compared with the Doppler broadening $W_{\rm Doppler}$ in hot WD atmospheres: We have examined their variation with the atmospheric layer temperatures and with the Rosseland optical depth for different atmospheric models of Wesemael (1981) ($T_{\rm eff} = 7 \times 10^4$ to 10^5 K and $\log g = 6$–9). We found that, for all the plasma conditions of DO WD atmospheres, the Stark broadening is more important than the Doppler one. The accurate Stark broadening parameters for the two strontium ions will be of interest for the investigation of hot WDs and for the determination of the strontium abundance in such stars. We hope that our results can fill the lack of Stark broadening data for these two ions in the data base STARK-B and can be used for the plasma diagnostic of the studied stars.

ACKNOWLEDGEMENTS

HE would like to thank the Deanship of Scientific Research at Umm Al-Qura University for supporting this work by grant code: (22UQU4331237DSR01).

This work was supported by the Tunisian Laboratoir de Spectroscopie et Dynamique Moléculaire (LR18ES02) and the French Laboratoire d'Etudes du Rayonnement et de la Matière en Astrophysique et Atmosphères (LERMA)- Unité Mixte de Recherches (UMR) 8112, of the Paris Observatory and the Centre National de la Recherche Scientifique (CNRS). We also acknowledge financial support from the 'Programme National de Physique Stellaire' (PNPS) of CNRS/Institut national des Sciences de l'Univers (INSU), Commissariat à l'Energie Atomique (CEA), and Centre National d'Etudes Spatiales (CNES), France.

DATA AVAILABILITY

The data underlying this article are available in the article and in its online supplementary material available at CDS via anonymous ftp to cdsarc.u-strasbg.fr (130.79.128.5) or via https://cdsarc.unistra.fr/viz-bin/cat/J/MNRAS.

REFERENCES

Albert D. et al., 2020, Atoms, 8, 76
Aloui R., Elabidi H., Sahal-Bréchot S., Dimitrijević M. S., 2018, Atoms, 6, 20
Aloui R., Elabidi H., Hamdi R., Sahal-Bréchot S., 2019a, MNRAS, 484, 4801
Aloui R., Elabidi H., Sahal-Bréchot S., 2019b, J. Quant. Spectrosc. Radiat. Transfer., 239, 106675
Aloui R., Elabidi H., Sahal-Bréchot S., 2020, Contrib. Astron. Obs. Skalnaté Pleso, 50, 154
Aloui R., Elabidi H., Sahal-Bréchot S., 2021, Eur. Phys. J. D, 75, 218
Baranger M., 1958, Phys. Rev., 112, 855
Bethe H. A., Salpeter E. E., 1957, Quantum Mechanics of One–and Two–Electron Atoms. Springer, Berlin
Charro E., Martín I., 1998, A&AS, 131, 523
Cowley C. R., 1971, The Observatory, 91, 139
Dimitrijević M. S., 2003, Astron. Astrophys. Trans., 22, 389
Dimitrijević M. S., 2020, Data, 5, 73
Dimitrijević M. S., Sahal-Bréchot S., Bommier V., 1991, A&AS, 89, 581
Dimitrijević M. S., Ryabchikova T., Popović L. Č, Shulyak D., Khan S., 2005, A&A, 435, 1191
Eissner W., 1998, Comput. Phys. Commun, 114, 295
Eissner W., Jones M., Nussbaumer H., 1974, Comput. Phys. Commun., 8, 270
Elabidi H., 2021, MNRAS, 503, 5730
Elabidi H., Sahal-Bréchot S., 2019, MNRAS, 484, 1072
Elabidi H., Ben Nessib N., Sahal-Bréchot S., 2004, J. Phys. B: At. Mol. Opt. Phys., 37, 63
Elabidi H., Ben Nessib N., Cornille M., Dubau J., Sahal-Bréchot S., 2008, J. Phys. B: At. Mol. Opt. Phys., 41, 025702
Elabidi H., Ben Nessib N., Sahal-Bréchot S., 2008, Eur. Phys. J. D, 54, 51
Gailitis M., 1963, J. Exp. Theor. Phys., 17, 1328
Grant I. P., 1988, in Wilson S.ed., Relativistic Atomic Structure Calculations.. Methods in Computational Chemistry, Springer, Boston, MA
Grant I. P., McKenzie B. J., Norrington P. H., Mayers D. F., Pyper N. C., 1980, Comput. Phys. Commun., 21, 207
Kramida A., Ralchenko Yu., Reader J., NIST ASD Team, 2021, NIST Atomic Spectra Database (ver. 5.9). National Institute of Standards and Technology, Gaithersburg, MD
O'Sullian G., 1989, J. Phys. B: At. Mol. Opt. Phys., 22, 987
O'Sullian G., Maher M., 1989, J. Phys. B: At. Mol. Opt. Phys., 22, 377
Persson W., Pettersson S. G., 1984, Phys. Scr., 29, 308
Rauch T. et al., 2007, A&A, 470, 317
Rauch T., Quinet P., Hoyer D., Werner K., Demleitner M., Kruk J. W., 2016a, A&A, 587, A39
Rauch T., Gamrath S., Quinet P., Löbling L., Hoyer D., Werner K., Kruk J. W., Demleitner M., 2017a, A&A, 599, A142
Rauch T. et al., 2017b, A&A, 606, A105
Rauch T. et al., 2020, A&A, 637, A4
Roueff E., Sahal-Bréchot S., Dimitrijević M. S., Moreau N., Abgrall H., 2020, Atoms, 8, 36
Sahal-Bréchot S., Elabidi H., 2021, A&A, 652, A47
Sahal-Bréchot S., Dimitrijević M. S., Moreau N., 2020, J. Phys. Conf. Ser., 1412, 132052
Sahal-Bréchot S., Dimitrijević M. S., Moreau N., 2022, STARK-B data base, Available at: http://stark-b.obspm.fr (accessed 30 January 2021)
Sansonetti J. E., 2012, J. Phys. Chem. Ref. Data, 41, 013102
Saraph H. E., 1978, Comput. Phys. Commun, 15, 247
Werner K., Rauch T., Knörzer M., Kruk J. W., 2018, A&A, 614, A96
Werner K., Rauch T., Kruk J. W., 2018, A&A, 609, A107
Wesemael F., 1981, ApJS, 45, 177
Wyart J. F., Artru M. C., 1989, Phys. Lett. A, 139, 8

SUPPORTING INFORMATION

Supplementary data are available online at CDS via anonymous ftp to cdsarc.u-strasbg.fr (130.79.128.5) or via https://cdsarc.unistra.fr/viz-bin/cat/J/MNRAS.

Table 3. Current spontaneous transition probabilities A_{ij}, weighted oscillator strengths *gf*, and line strengths *S* for Sr V allowed transitions.

Table 4. Current spontaneous transition probabilities A_{ij} compared with the experimental results (Exp) of Sansonetti (2012), weighted oscillator strengths *gf* compared with the MCDF results of O'Sullian (1989) using the MCDF code of Grant et al. (1980), and line strengths *S* for Sr VI allowed transitions.